Silva, T. P., De Oliveira, D. V., Veiga, J. P., Ávila, P. F., Candeias, C., Salas-Colera, E., & Caldeira, R. (2019). Mineralogy and chemistry of incrustations resulting from the 2014–2015 eruption of Fogo Volcano, Cape Verde. Bulletin of Volcanology, 81(4).

DOI: 10.1007/s00445-019-1282-0

Mineralogy and chemistry of incrustations resulting from the 2014-15 eruption of Fogo volcano, Cape Verde

Teresa P. Silva[1*], Daniel P. S. de Oliveira[1], João P. Veiga[2], Paula Ávila[3], Carla Candeias[4], Eduardo Salas-Colera[5], Rita Caldeira[6]

[1] Mineral Resources and Geophysics Research Unit, National Laboratory for Energy and Geology (LNEG), Estrada da Portela, Apartado 7586, 2610-999 Amadora, Portugal

[2] CENIMAT/I3N, Departamento de Ciência dos Materiais, Faculdade de Ciências e Tecnologia, Universidade NOVA de Lisboa, 2829-516 Caparica, Portugal

[3] Mineral Science and Technology Unit, National Laboratory for Energy and Geology (LNEG), S. Mamede de Infesta, Portugal

[4] EpiUnit - Epidemiology Research Unit, Environmental Health Department, Institute of Public Health of the University of Porto, Porto, Portugal / GeoBioTec - Geobiosciences, Geotechnologies e Geoengineering Research Center, Geosciences Department, University of Aveiro, Aveiro, Portugal

[5] SpLine, Spanish CRG Beamline, European Synchrotron Radiation Facility (ESRF), Grenoble, France / Instituto de Ciencia de Materiales de Madrid-CSIC, Madrid, Spain

[6] Geology, Hydrogeology and Coastal Geology Unit, National Laboratory for Energy and Geology (LNEG), Amadora, Portugal

Corresponding author*: teresa.pena@lneg.pt; Tel: +351210924600

Acknowledgments This research received financial support from FCT (Fundação para a Ciência e Tecnologia) through project FIRE (PTDC/GEO-GEO/1123/2014). We acknowledge the European Synchrotron Radiation Facility for provision of synchrotron radiation facilities and in particular in using beamline BM 25A. Special thanks are due to the guides Manuel Montrond Fernandes (Izaquiel) and Edimar Montrond that helped us in the Fogo volcano. J.P. Veiga acknowledges funding by FEDER funds through the COMPETE 2020 Programme and National Funds through FCT-Portuguese Foundation for Science and Technology under the project UID/CTM/50025/2013 and the funding from the European Union Horizon 2020 research and innovation programme H2020-DRS-2015 GA nr. 700395 (HERACLES project). Special thanks are also due to Dr. Tonči Balić-Žunić, an anonymous reviewer and to the editors for their comments on the manuscript. We are also grateful to Dr. Lídia Quental for the satellite image of Fogo Island.

Abstract The last eruption of the Fogo volcano, in the Cape Verde Archipelago, occurred in 2014-15. A mineralogical and chemical study was undertaken on fumarole incrustations resulting from this event and compared with results obtained from the previous 1995 eruption. The mineralogical constitution of the fumarole deposits was assessed by X-ray diffraction and the chemical characterization was performed through X-ray fluorescence spectrometry with a wavelength dispersive system and by energy dispersive X-ray fluorescence at the European Synchrotron Radiation Facility. The most represented compounds/minerals in solid deposits were sulphur, sodium chloride, and calcium sulphates with variable degrees of hydration, sodium sulphate, hydrated sulphates of sodium aluminum, potassium magnesium, or sodium magnesium and a fluorine-bearing mineral. Thenardite (Na_2SO_4) and its polymorph (phase III) were found simultaneously for the first time in incrustations, to the best of our knowledge. A large span of minor and trace elements present in incrustations (Na, Mg, Al, Si, P, S, Cl, K, Ca, Ti, V, Mn, Fe, Ni, Cu, Zn, As, Se, Br, Rb, Sr, Y, Zr, Nb, Mo, Ba, Ce, Tl, Pb) were also identified, some of them potentially hazardous to animal and human health. This study reveals that low temperature incrustations, allied to the atmospheric conditions of Fogo volcano, constitute a natural laboratory to observe the process of mineral formation - namely, the Na_2SO_4 phase III considered metastable.

Keywords Fogo volcano; Cape Verde; Fumaroles; Incrustations; Volcanic gases; Minerals; Human and animal health

Introduction

75 The process of mineral formation can be observed in fumaroles at active volcanoes, i.e. in a
76 restricted space and time where the emanating hot gases are continuously depositing
77 compounds/minerals. Gases released from the magma are rich in volatile components such as
78 H_2O, CO_2, SO_2, H_2S, HCl, HF, H_2, CH_4 and CO, water vapour being the dominant constituent of
79 high temperature (>500^{0}C) volcanic gases (e.g. Symonds et al. 1994; Fischer 2008; Aiuppa
80 2015). Differences in the concentration distributions of these constituents are related to their
81 fractionation during magma degassing and to their sources in magmas, the composition of
82 volcanic gases being dependent on the temperature at fumaroles (Giggenbach 1996; Zelenski and
83 Taran 2011). Recent studies on arc-volcanic gases have shown magmatic fluid uniformity in
84 both the water isotopic composition and Cl content, as well as in the total composition (H–C–O–
85 S–Cl–F), that contrast with volcanic fluids of non-arc volcanoes (De Moor et al. 2013; Paonita et
86 al. 2013; Shinohara 2013; Taran and Zelenski 2015).
87 Volatile species transported by hot volcanic gases, either pure or resulting from their
88 interaction with their hydrothermal surroundings, emitted through vents and fissures, are
89 deposited or released to the atmosphere at the emitting source (Symonds et al. 1987). The
90 material deposition formed by cooling and condensation or sublimation - fumarole incrustations
91 - generates a coloured field and constitutes an indication of the role played by magmatic fluids in
92 the processes of mineral formation (e.g. Lacroix 1907; Stoiber and Rose 1974; Óskarsson 1981,
93 1984; Toutain et al. 1990). These studies have all shown that incrustations retain a significant
94 amount of the transported components that are carried in the minerals as nanometer-sized
95 inclusions. For example, the 1902 eruption of Santa Maria, Guatemala, was one of the largest
96 volcanic eruptions of the 20th century (Williams and Self 1983). New eruptions began in 1922
97 (Rose 1973), and studies performed between 1964 and 1969 on condensates from Central
98 American volcanoes (including the dome that began to grown within the Santa Maria caldera:
99 Santiaguito) showed that condensate chemistry depended on fumarole location and time of

collection relative to the eruptive and cooling history of the emplacement event (Stoiber and Rose 1970). The most abundant and frequently found minerals in incrustations were sulphur, hematite, halite, sylvite, gypsum, ralstonite, anhydrite, thenardite and langbeinite (Stoiber and Rose 1974). Other examples could be cited: sulphur, opaline silica, gypsum, ralstonite and thenardite at Hawaiian volcanoes (Naughton et al. 1976); gypsum, anhydrite, sulphur, tridymite, halite and soda alum at Mount St. Augustine, Alaska (Kodosky and Keskinen 1990) and the extensive work of fumarolic minerals at European volcanoes completed by Balić-Žunić et al. (2016a). The description of fumarole products resulting from low temperature volcanic emissions, including iron, magnesium, aluminum, and manganese chlorides (Pelloux 1927) as well as sulphur and realgar at Vesuvius have also been recorded. Yellow amorphous iron chloride, cristobalite, and minor amounts of ralstonite (60-80°C), soda-alum (150°C) - or even anhydrite and sodium aluminum sulphate (350°C) in one fumarole of Santiaguito volcano (Stoiber and Rose 1969) have also been noted. Sulphur, gypsum, alunogen, and other hydrous sulphates in European fumarolic systems are well-documented by Balić-Žunić et al. (2016a).

Studies have also been completed on incrustations left at systems active in the Atlantic Ocean, including: Iceland, Azores, Canary Islands, Tristan da Cunha and on the island of Fogo in the Cape Verde Archipelago (e.g. Baker et al. 1964; Figueiredo et al. 1997; Jakobsson et al. 2008; Melián et al. 2012; Carvalho et al. 2014). In each case the incrustations provide indirect sources of information on the nature of volcanic degassing and, particularly, on heavy metal transport by lava degassing (Toutain et al. 1990). A detailed knowledge of the nature and range of heavy elements carried by gases emanating from fumaroles following a volcanic eruption, or during periods of unrest, is vital in the domains of environment, geochemistry and volcano risk assessment (e.g. Chiodini et al. 1995, 2002; Africano et al. 2002; Orlando et al. 2011). Frequently, elements such as Hg, Pb (Ferrara et al. 1995) and the highly poisonous element Tl are present, and pose a significant threat to human (and environmental) health (Rodríguez-

Mercado and Altamirano-Lozano 2013). This feature was noticed following the 1995 eruption of Fogo volcano and was studied by synchrotron X-ray microprobe (Figueiredo et al. 1999). In spite of this finding, little information exists about the mineralogy and chemistry related to fumarole deposits, and about the chemical composition of gases emitted, by Fogo and, in particular, during the last two eruptive periods (1995 and 2014-15).

To contribute to a better knowledge on the process of mineral formation at low temperature (<250^{0}C), we here present a mineralogical study performed on incrustations (materials formed by cooling and condensation or sublimation and deposited in the field around fumaroles) from the latest eruption of Fogo volcano. The occurrence of thenardite (Na_2SO_4) and its polymorph (phase III) in one single locality, represents, to the best of our knowledge, the first discovery of both of these phases occurring simultaneously. We discuss this particular observation in terms of transition temperatures and phase stabilities. Finally, the comparison with minerals resulting from the previous eruption (1995) is undertaken. Moreover, the chemical study based on these materials is used to infer the volcanic gas' composition in terms of their heavy metal contents and toxicity.

Geological setting

Fogo Island, part of the Cape Verde Archipelago (Fig. 1), is the only island in the archipelago with known historic volcanic activity, since the discovery of the archipelago in the 15th century as registered in logs of ships (Ribeiro 1998). The island was formed in an oceanic environment by a mantle plume - hot-spot type mechanism (Mata et al. 2017). Volcanism is essentially alkaline and it is assumed that Fogo is currently located above a hot-spot (Torres et al. 1995, 1997; Silva et al. 1997).

Fogo Island is nearly circular in shape approximately 25 km in diameter with a maximum altitude of 2829 m a.s.l., corresponding to a central volcano with its centre offset to the NE to a lateral east flank collapse (Day et al. 1999; Maccaferri et al. 2017). Fogo also has more than one hundred adventive cones, 50 to 100 m high, distributed across the flanks of the main eruptive cone and summit caldera - Chã das Caldeiras. This caldera is approximately 9 km in N-S diameter, and whose steep back wall - Bordeira - reaches 1 km in height. Within this caldera the 1100 m high cone of the Pico do Fogo volcano (currently the highest point on the island), with a crater 100 to 200 m deep and 500 m in diameter was built; its first activity is unknown, but after the second half of the 18th century the eruptive occurrences begun at the adventive cones (Torres et al. 1997; Ribeiro 1998).

The most recent eruptive events occurred in 1995 and 2014-15, both of which produced extensive lava flow fields (a'a and pahoehoe) at Chã das Caldeiras, which destroyed houses and agricultural land (Jenkins et al. 2017). The local population was about 1200 inhabitants in 2014, and the economy was based on agriculture (mainly vine and fruit plantations), grazing, and tourism (Vieira et al. 2017). The latest eruption (November 23, 2014 to February 7, 2015) occurred on a NE-SW trending 700 m-long fissure located on the SE flank of the previous 1995 cinder cone, an adventive vent developed on the SW flank of the younger Pico do Fogo volcano (Fig. 2). The 2014-2015 eruption was more explosive than the one in 1995, varying from Hawaiian to Strombolian and Vulcanian activity phases, which sometimes occurred simultaneously at the different aligned craters. Lava flow simulations have been carried out to better understand the 2014-2015 lava flow crisis and to prepare for the next inevitable eruption (Richter et al. 2016).

Experimental

175

176 Sampling

177

178 Two sampling campaigns were carried out (Table 1 and Fig. 1). In November 2016 we collected
179 rocks (basaltic lava) and incrustations deposited on rocks from near the 2014-15 main vent (Figs.
180 3 and 4), while in February 2017 we recorded the temperatures in the area around the samples
181 with a digital thermometer using a thermocouple type "K" - Chromel-Alumel (Metra
182 Instruments, http://www.metra-instruments.com/PDF/6504.pdf).

183 Adjacent to the main vent (Fig. 3), the fumaroles were almost imperceptible in both field
184 campaigns. Yellow - sulphur - (Fig. 5a) and white precipitates/sublimates were deposited in the
185 field as well as orange-red altered rocks. White incrustations were collected along the walls of a
186 higher-temperature unstable fracture (Fig. 5b). The highest registered temperature (238°C) was
187 measured in a hole (Fig. 5c) containing white material (collected near the surface), in alignment
188 with the fracture and probably connected to it.

189 There is a second, smaller vent, called by the local population "vulcãozinho" (little volcano),
190 located at lower altitude than the main one (Figs. 1, 6 and 7). It has a pit created by the eruption
191 in which white incrustations were found deposited on the rocks. A big tunnel, which also
192 contains white incrustations, enters the bottom of the pit, from which lava came out at the
193 beginning of the eruption, before being swallowed by the pit.

194

195 Methods and techniques

196

197 A Philips PW 1500 powder diffractometer with Bragg-Brentano geometry, equipped with a
198 large-anode copper tube operating at 50 kV - 40 mA and a curved graphite crystal
199 monochromator, was used to collect X-ray diffraction (XRD) patterns of the powdered samples

200 previously observed using a stereomicroscope (Zeiss, Stemi SV-11). The images were collected
201 with a digital Zeiss camera (Axio-Cam Mrc). An effort was made to select pure phases of
202 incrustations with respect to the morphology and colour, avoiding contamination by minute lava
203 fragments. The thermodynamic conditions which prevail during the deposition of minerals from
204 volcanic gases favor the formation of predominantly fine-grained, dispersed, cryptocrystalline
205 and, in some exceptional cases, imperfect crystalline aggregates (Vergasova and Filatov 2016).
206 The identification of fumarole minerals was in some cases difficult due to the presence of a
207 mixture of phases and uncommon mineral associations.

208 For this reason a semi-quantitative chemical analysis through X-ray fluorescence
209 spectrometry with wavelength dispersive system (XRF-WDS) was performed. For the elemental
210 analysis, a PANalytical AXIOS sequential spectrometer (Rh X-ray tube, 4 kW) under He flow
211 was used. Samples were analyzed in powder form to avoid chemical heterogeneities and
212 crystalline effects. Standardless semi-quantitative analysis was performed with the SuperQ IQ+
213 software package (Figueiredo et al. 2018).

214 As a preliminary approach, the chemical composition of four incrustation samples was also
215 obtained by energy dispersive X-ray fluorescence (EDXRF) at the European Synchrotron
216 Radiation Facility (ESRF) in Grenoble/France. The experiments were performed with the
217 instrumental set up of beamline BM 25A, using an excitation energy of 29.58 keV (powdered
218 samples were placed between two Kapton foils, a special pure adhesive tape that reduces
219 interference from any support material) and an irradiated area of 1 mm^2. A Sirius Si(Li) 13-
220 element fluorescence detector was employed for EDXRF experiment. Si(Li) crystals have a good
221 spectral response over an energy range between 2-30 keV. The high brilliance of synchrotron X-
222 rays allows for remarkably low limits of detection for most chemical elements, thus enabling the
223 analysis of trace and sub-trace species hosted by a mineral (provided the medium atomic number

of the major components is relatively low). The energy dispersive spectra collected over a period of 300 s for each sample were fitted using the PyMca software (Solé et al. 2007).

Results

Mineralogical characterization

The mineralogical composition of the incrustations was obtained by XRD (Table 2), after careful selection using a stereomicroscope (illustrative images can be observed in Fig. 8). However, some phases such as olivine, pyroxene and titanite are attributed to basaltic lava. More than one phase was identified for the majority of samples, with the first one being the most representative for each sample assigned in Table 2.

Out of interest, sample F20/17 is a whitish powder that the local population usually uses to treat certain diseases (called "scontra"), and it is also sold to tourists. XRD analysis of this sample showed the presence of a mixture of anhydrite ($CaSO_4$) and gypsum ($CaSO_4.2H_2O$) with vestigial sulphur.

The main phases identified in the incrustations were sulphur (common orthorhombic form, α-S), sodium chloride (halite, NaCl), calcium sulphates with variable degrees of hydration (anhydrite, $CaSO_4$, bassanite, $CaSO_4.1/2H_2O$ and gypsum, $CaSO_4.2H_2O$), anhydrous sodium sulphate (thenardite and Na_2SO_4 (III)), sodium aluminum sulphate hydrate (tamarugite, $NaAl(SO_4)_2.6H_2O$), potassium magnesium sulphate hydrate (picromerite, $K_2Mg(SO_4)_2.6H_2O$), sodium magnesium sulphate hydrate (bloedite, $Na_2Mg(SO_4)_2.4H_2O$), or with more metallic elements (bianchite, $(Zn_{0.69}Fe_{0.21}Mg_{0.10})SO_4.6H_2O$) and a fluoride (ralstonite, $Na_xMg_xAl_{1-x}(F,OH)_3.(H_2O)n$).

249

250 Chemical analysis

251

252 The semi-quantitative results obtained by XRF-WDS for selected powder samples (Table 3) are
253 in accordance with the main mineralogical phases identified. Sulphur samples are quite pure. The
254 highest Mg contents belong to samples of bloedite and picromerite (9%) and bianchite (7%). The
255 K contents of between 18 and 27% correspond to picromerite, and of around 10% to ralstonite.
256 As expected, the higher levels of Ca and Sr belong to incrustations with anhydrite, bassanite and
257 gypsum. Samples of altered rock (basaltic lava) are rich in the heavy elements Zr, Ba, Ce, Tl, as
258 well as Ti and Fe (F12-powder scraped off the rock, F14-red rock and F27-yellow and orange
259 incrustations).

260 The comparison of EDXRF spectra (Fig. 10) shows that Se is carried by massive S, and As is
261 present in four samples, with the highest values being in the anhydrite and gypsum mixtures
262 (F20-white incrustations, aggregate and disaggregate). Br is present in the halite sample (F19). In
263 addition, low concentrations (traces) of the following elements can be detected: Pb, Rb, Sr, Y,
264 Zr, Nb and Mo, especially in F20 samples (the intensity of the lines close to the excitation energy
265 is increased). The presence of lithophile elements like Rb, Sr, Y, Zr and Nb is possibly due to
266 minor silicate phases. The low detection limits also make it possible to identify Cu and Zn.

267 A large span of minor and trace elements was identified by combining both techniques (Na,
268 Mg, Al, Si, P, S, Cl, K, Ca, Ti, V, Mn, Fe, Ni, Cu, Zn, As, Se, Br, Rb, Sr, Y, Zr, Nb, Mo, Ba, Ce,
269 Tl, Pb), which were present in incrustations deriving from the condensation and sublimation of
270 volcanic gases (though it cannot be excluded that some elements might result from lava
271 impurities).

272

273

Discussion

Low temperature incrustations

Incrustations can be grouped according to the mineralogy in terms of elemental sulphur, sulphates and halides. The species distribution around the main vent (Tables 1 and 2) shows that sulphur was dominant, but anhydrite, bassanite, gypsum, thenardite, bloedite, tamarugite, picromerite, ralstonite and halite were also found at about 70^0C and about 160^0C. There was also crystallized anhydrite and bassanite on the walls of one E-W fracture (182^0C) located around 20m from the main vent (see Figs. 2b and 5b). Halite and thenardite, and its polymorph (phase III), were identified inside a pit (238^0C) located near to the 1995 cinder cone, around 80m away from the main vent (Fig. 2b). At a smaller vent located at lower altitude (Fig. 6) only thenardite and halite were found.

Sulphur was present as an orthorhombic mineral in the form of yellow hyaline crystals and massive aggregates. The common, stable sulphur (α-S), which is very frequent in volcanic areas, is constituted of S_8 molecules. Due to the molecular character of the chemical bonding in native sulphur, the up-take of other elements during crystallization is extremely selective, with only Se and possibly As being capable of being retained in solid solution (Figueiredo et al. 1999).

Sulphate phases are dominated by common anhydrite (β-$CaSO_4$), bassanite and gypsum. Anhydrite is associated with bassanite, hemihydrate (e.g. sample F18/17, T=182°C) or with gypsum. The metastable polymorph γ-$CaSO_4$ (soluble anhydrite) obtained by slow dehydration of gypsum or hemihydrate at 100°C is hexagonal and its transformation to anhydrite begins at 150°C (Flörke 1952). In natural samples it is known that gypsum coexists with anhydrite along with minor amounts of alkali and alkaline halide impurities and that the equilibrium temperature of the gypsum-anhydrite phase is lowered due to the presence of impurities that prevent the free

movement of water molecules. The transition of gypsum to bassanite is associated with a rearrangement of sulphate ions, but such changes are marginal during the transition of bassanite to anhydrite (Prasad et al. 1998). Sodium chloride solutions promote a step-wise dehydration process and a decrease in the temperature of gypsum-bassanite-anhydrite transformation (Hardie et al. 1967; Prasad et al. 1998). However, halite was not found associated with calcium sulphate minerals in Fogo volcano. Bassanite occurrence in fumaroles is not as common as anhydrite or gypsum, but has also been referenced (Balić-Žunić et al. 2016a).

Tamarugite was only found at the main vent as a white material (e.g. sample F17/17, T=76.5°C) with bianchite. This mineral has been described as occurring at Vulcano, Italy (Lombardi and Sposato 1981) and at Te Kopia, New Zealand (Mackenzie et al. 1995). Bloedite and picromerite were found together at the main vent, associated with thenardite and halite. Of the minerals identified, thenardite occurs in a particular situation and is thus treated in a separate section.

The presence of Cl was found only in halite, which occurred in a pit with the highest temperature registered (238°C) at the main vent (sample F19/17), and also at the smaller vent "vulcãozinho" (sample F24/17). In both cases, halite was associated with thenardite unlike what was noticed in previous eruption (Silva 1999).

The observed mineral associations are spatially confined to different zones in the field, and provide evidence of the distinctive features of the gas compositions that arrive at the surface (gases of the S, Cl, and F group, and water vapour). The interaction between fluorine-bearing gases and volcanic rocks gives rise to a more or less superficial discoloration of the pyroclastic material and the formation of ralstonite (brownish in colour). This mineral was found for the first time in Ivigtut (Greenland) and described by Brush in 1871 (Palache et al. 1951). Ralstonite has frequently been observed in other fumarole incrustations: for instance, Rosenberg (1988) mentions the existence of three hydrated aluminum fluorides in incrustations from Mount Erebus

(Antarctica), including ralstonite. Rosenberg also notes that F-rich volcanic gases are associated with alkaline volcanoes, as is the case of Fogo volcano. Ralstonite was identified in this study (e.g. sample F27/17) and in the previous eruption (1995) incorporating an orange gel (Figueiredo 1997). Although fluorine was not chemically detected, since it is a very light element, its presence is clearly indicated by ralstonite, indicating that HF is a possible gaseous component. HF has also been described as a constituent of the volcanic ash and as contributing to environmental hazards (Cronin et al. 2003).

Thenardite and phase III polymorph

Thenardite occurs associated with bloedite and picromerite around the main vent, and with halite at the smaller vent "vulcãozinho", while sodium sulphate (phase III) was identified in sample F19/17, along with thenardite and halite (Fig. 9), collected on the upper part of the pit walls with a temperature of 238°C (Fig. 5c).

This sodium sulphate with five polymorphs has been found as precipitates around fumaroles elsewhere, e.g. in Tolbachik volcano (Pekov et al. 2014) and Kudriavy volcano, Kurile Islands (Wahrenberger et al. 2002) in Russia, and on the "Cueva Del Tigre" lava tube, Argentina (Benedetto et al. 1998). Na_2SO_4 exhibits a variety of phase transitions between its five anhydrous polymorphs (labelled I–V, according to Kracek, 1929). The phase stability, transition temperatures and structures have been studied by many authors (e.g. Mehrotra et al. 1975; Rasmussen et al. 1996; Vidya and Lakshminarasappa 2013; Taide et al. 2015) and the phase transformation sequence can be described as $V \leftrightarrow^{200°C} III \leftrightarrow^{230°C} II \leftrightarrow^{237°C} I \leftrightarrow^{883°C}$ melt. Na_2SO_4 forms two naturally occurring minerals: mirabilite ($Na_2SO_4.10H_2O$) and thenardite (Na_2SO_4). At room temperature, phase V (thenardite) is known to be stable while phase III is metastable. Phases I and II are high-temperature polymorphs, and phase II has a narrow stability zone. Phase

IV is considered to be metastable (Taide et al. 2015). In the high-temperature polymorph, Na_2SO_4 (I), up to 30% cation vacancies can be generated by substitution of Na^+ by bi- and trivalent ions (Eysel et al. 1985). Recently, a new mineral, metathenardite [high-temperature hexagonal polymorph, Na_2SO_4 (I)], was approved by the International Mineralogical Association, Commission on New Minerals, Nomenclature and Classification (IMA 2015-102) as a dimorph of thenardite (Pekov et al. 2016). Choi and Lockwood (2005) found that phase III remains stable for more than one year at room temperature in dried air, but in the normal atmosphere, phase III slowly reverts to phase V, while for Bobade et al. (2009) the transformation sequences of Na_2SO_4 while cooling (I→III→V) and heating (V→I) in ambient conditions are different.

To the best of our knowledge, this is the first time that thenardite and Na_2SO_4 (phase III) have been found simultaneously in incrustations. Fogo volcano has different atmospheric conditions from those previously used in the study of these minerals, due to the occurrence of summer rainfall at the beginning of autumn and only rare cloudbursts during the rest of the year, as well as low relative humidity (RH). These conditions allow the initial mineralogical phases to be conserved for a longer time before hydration or phase transition takes place. On the contrary, fumarole products from Vesuvius, some of them important due to their rarity, are subject to rapid alteration or, since they are quite soluble, are quickly carried off by rain shortly after their formation (Pelloux 1927).

The results of experiments, performed under various RH conditions, on sodium sulphate crystallization at room temperature (Rodriguez-Navarro et al. 2000), along with the arguments of Brodale and Giauque (1972) that although phase III is thermodynamically unstable at all temperatures it can exist indefinitely if kept dry, support our observations. In reality, the first authors studied the system Na_2SO_4-H_2O, namely the two phases considered stable at room temperature, thenardite and mirabilite. With high evaporation rate conditions (low RH), they

observed the precipitation of thenardite directly from the saturated solution at temperatures below 32.4^{0}C (transition point of mirabilite-thenardite). At very low RH conditions (below 15%), occasionally they found crystals of thenardite (V) with a small amount of phase III (without formation of mirabilite), being the heterogeneous nucleation of thenardite in a supersaturated solution, the reason for its formation at temperatures below the transition point. Mirabilite was never found in incrustations from Fogo volcano; the low RH and high fast evaporation conditions explains the co-existence of Na_2SO_4 (V) and phase III in the same sample. These two phases are both metastable at 244^{0}C and they are in equilibrium at that point, as shown by the free energy diagrams of Brodale and Giauque (1972); the stability of phase III at lower temperatures is possible for long times in a dry environment, being RH a key factor for that permanence as also shown by Linnow et al. (2006).

Considering that thenardite has been used in many applications, such as for thermal energy storage (Vidya and Lakshminarasappa 2013), and that sodium sulphate is the most widely used salt in accelerated weathering tests of natural rocks and building materials (Rodriguez-Navarro et al. 2000; Steiger and Asmussen 2008), the present data are important to complement the previously recorded transition temperatures and phase stability laboratorial studies. The co-existence of these two polymorphs is proof that Nature could produce what had been observed in strictly defined conditions in the laboratory (Linnow et al. 2006), as well as indicating that a high Na_2SO_4 supersaturated solution gave rise to the incrustations.

Comparison with previous eruptions

Comparing the mineralogical phases identified in incrustations resulting from the 2014-15 eruption of Fogo volcano with those found following the 1995 eruption (Figueiredo 1997; Figueiredo et al. 1997), shows that some minerals are common to both eruptions (sulphur,

399 gypsum, anhydrite, halite, ralstonite). Others, however, were only identified in the 1995 event,
400 namely alums, $MAl(SO_4)_2.12H_2O$, both sodic (M=Na) and potassic (M=K), halotrichite
401 ($FeAl_2(SO_4)_4.22H_2O$), and sylvite (KCl) - only associated with halite and occasionally "soluble
402 anhydrite" (γ-$CaSO_4$); natrojarosite ($NaFe_3(SO_4)_2(OH)_6$) was also identified in association with
403 others minerals (Silva 1999), and an orange gel with minute, dispersed white grains (ralstonite).
404 This amorphous, highly hygroscopic gel was heated to 600^0C, resulting in the loss of volatile
405 constituents (mainly Cl and Tl) and in the formation of litharge (red PbO) together with a
406 multiple oxide with bixbyite-type crystal structure (Figueiredo 1997).
407 Two distinct zones resulting from the 1995 eruption characterized the fumarole field (Silva
408 1999): one of high temperature (>600°C) with only white incrustations (mainly halite and more
409 rarely sylvite), and another one with lower temperatures (between 85^0C and around 500^0C), in
410 which the other minerals above mentioned were abundant. The observation of a zone in which
411 there were only volcanic gases rich in chlorine raised the question as to whether there was an
412 input of sea water into the magmatic chamber, although no studies were performed to investigate
413 this hypothesis (Silva 1999); however, descriptions in Ribeiro (1998) relating to material of the
414 1785 Fogo eruption indicated the same idea. Halite and sylvite were not found associated with
415 other minerals during the 1995 eruption of Fogo. This is contrary to the observations of other
416 authors who found minerals as fumarole incrustations in silica-tubes (e.g. Stoiber and Rose 1974;
417 Le Guern and Bernard 1982; Symonds et al. 1987; Quisefit et al. 1989; Toutain et al. 1990;
418 Symonds et al. 1992), including the 2014-15 sampling of Fogo (this work).
419 In addition to the above mentioned mineral species, sampling of the 1995 incrustation field,
420 carried out in mullite tubes (Silva 1999), revealed anhydrite, steklite ($KAl(SO_4)_2$) and
421 millosevichite ($Al_2(SO_4)_3$) in the lower part of the tubes (around 500^0C) and alunogen
422 ($Al_2(SO_4)_3.16H_2O$) in the upper part. Conversely, the presence of alunogen (upper part of the
423 tubes) and K-alum (field) along with Na-alum, halotrichite and the orange gel suggests a high

RH at the time of sampling (it rained around that time on the island), in apparent opposition to the observed anhydrous species.

The 2014-15 eruption created a lower temperature fumarole field (<250^{0}C), formed by incrustations of sulphur, halite, anhydrite, bassanite, gypsum, thenardite and its polymorph (phase III), tamarugite, picromerite, bloedite, bianchite and ralstonite, minerals which are comparatively less hydrated than those identified for the previous eruptive event, probably due to lower RH and temperature. For instance, the dehydration of K-alum proceeds from crystalline $KAl(SO_4)_2.12H_2O$ to amorphous phases, and then to crystalline $KAl(SO_4)_2$ at around 240^{0}C (Kishimura et al. 2015). Conversely, Na-alum dehydrates directly to tamarugite without giving rise to the intermediate mendozite phase ($NaAl(SO_4)_2.11H_2O$) (Fang and Robinson 1972). The recognition of the unnamed phase, $NaAl(SO_4)_2$, in Santiaguito (Stoiber and Rose 1974) led us to suppose that tamarugite could result from the hydration of that phase instead of from a solution of sodium sulphate plus aluminum sulphate.

Volcanic gas composition

Based on the mineralogy and chemistry data for the incrustations, Ca is the major cation present; the low temperature of fumaroles allied to the presence of fluorine gas (indicated by the occurrence of ralstonite) suggest its provenance from both degassing of Ca-rich magma and a possible wall-rock input (Africano and Bernard 2000). It is thought that the metals Na^+, K^+, Mg^{2+} and Ca^{2+} degas from the magma as chlorides (e.g., NaCl, KCl, $MgCl_2$ and $CaCl_2$) (Martin et al. 2010). The origin of sulphate aerosols was assumed to be the slow oxidation of gaseous SO_2, but studies by Allen et al. (2002) showed that these particles could be emitted directly from volcanic vents. SO_2, H_2S, H_2, CO_2 and H_2O emission rates were measured before (Dionis et al. 2015a), and during the 2014-15 eruption, representing the first SO_2 plume measurements ever carried out

449 during an eruption of this volcano (Hernández et al. 2015): an increase in the SO_2/H_2S ratio plus
450 a decrease in CO_2/SO_2 was observed, which is indicative of the injection of SO_2-rich hot
451 magmatic gases into the H_2S-rich hydrothermal system of Pico do Fogo volcano as reported by
452 Hernández et al. (plume emissions: 10,688 t d^{-1} of CO_2, 57 t d^{-1} H_2S, 18 t d^{-1} H_2 and 24,245 t d^{-1}
453 H_2O). However, the formation mechanism of gypsum can also include the action of sulphurous
454 volcanic gases on Ca-bearing rocks (Deer et al. 1967).
455 Some authors (references in Dionis et al. 2015b) proposed four phases for the geological
456 evolution of Fogo including the uplift of a seamount series composed of carbonatites and
457 alkaline basalts, and recent studies classified the erupted magmas as alkaline, tephrites and
458 phonotephrites (Mata et al. 2017). The occurrence of carbonatite rocks is very rare in an oceanic
459 setting; nevertheless, oceanic carbonatites have been reported at some islands of the Cape Verde
460 archipelago (e.g. Assunção et al. 1965; Silva et al. 1981; Martins et al. 2010) and their origin has
461 been linked to mantle plumes, composed of recycled oceanic crust plus carbonated sediments
462 (Doucelance et al. 2010 and references herein).
463
464 Toxic elements
465
466 From the elements identified in incrustations and altered rocks, some of them (e.g. As, Se, Tl,
467 Pb) may raise environmental concerns due to their toxicity, which is dependent on various
468 factors (Wu and Sun 2016). For example, the major inorganic forms of As include the trivalent
469 arsenite and the pentavalent arsenate. Exposure to As occurs orally (ingestion), by inhalation or
470 by skin contact. The toxic effects of As are highly influenced by its oxidation state and
471 solubility, as well as many other intrinsic and extrinsic factors, for example inorganic As^{3+} is 2-
472 10 times more toxic than As^{5+} (Tchounwou et al. 2012).

Conversely, Se is known for its toxicity (Lenz and Lens 2009), which develops via a complex cycle involving adsorption by soil components (clays and other particulate minerals) and subsequent incorporation into plants, where it can accumulate (Ellis and Salt 2003). In the natural environment, it occurs as an element (Se^0) with two allotropes, orthorhombic and monoclinic, as anions - selenide (Se^{2-}) and diselenide (Se_2^{2-}) - and as cations - selenite (Se^{4+}) and selenate (Se^{6+}). However, Se is also recognized as being an essential nutrient for animals, humans and microorganisms. The occurrence of such elements is a major health hazard concern as local populations use sulphur and white materials as treatment for some human and animal diseases (by mixing and drinking with water for example). To clarify the speciation state of Se and the nature of Se-carrier phase(s) on incrustations samples, an X-ray absorption spectroscopy study (XANES) using synchrotron radiation has been undertaken at the Se *K*-edge (Silva et al. 2018). Different situations were observed: Se^{6+} tetrahedral coordination, in a mixture of bassanite and anhydrite, due to the replacement of S by Se in SO_4 tetrahedra; Se^{4+} pyramidal coordination in ralstonite, where selenium is probably linked to oxygen; and Se^0 in a sulphur sample due to diadochic replacement of S by Se.

Conclusions

The fumarole incrustations resulting from the low temperature (<250^{0}C) degassing of Fogo volcano are mainly composed of sulphur and sulphates, plus halides (fluoride and chloride). In the two last eruptions (1995 and 2014-15), the mineral halite (NaCl) was identified in the higher temperature zone of the fumarole field, but in the more recent eruption it was associated with thenardite and a polymorph of Na_2SO_4 (phase III). To the best of our knowledge, this is the first time that thenardite and its polymorph have been reported as co-existing in incrustations,

probably due to the atmospheric conditions at Fogo volcano (summer rainfall at the beginning of autumn and only rare cloudbursts in the rest of the year creating low relative humidity) that are critical for the preservation and occurrence of these minerals. Also, this situation indicates that a high Na_2SO_4 supersaturated solution gave rise to the incrustations.

In addition to halite, thenardite and Na_2SO_4 (III), sodium, magnesium, potassium and calcium minerals were observed: tamarugite ($NaAl(SO_4)_2.6H_2O$), bloedite ($Na_2Mg(SO_4)_2.4H_2O$), ralstonite ($Na_xMg_xAl_{1-x}(F,OH)_3.(H_2O)n$), bianchite ($Zn_{0.69}Fe_{0.21}Mg_{0.10})SO_4.6H_2O$), picromerite ($K_2Mg(SO_4)_2.6H_2O$), anhydrite ($CaSO_4$), bassanite ($CaSO_4.1/2H_2O$), and gypsum ($CaSO_4.2H_2O$). The same mineral groups were found in the 1995 eruption, but different species were observed, namely alums, $MAl(SO_4)_2.12H_2O$, both sodic (M=Na) and potassic (M=K), and sylvite (KCl), all of which have been described in fumarole incrustations at other volcanoes.

Calcium is the major cation present, suggesting that its provenance is from degassing of Ca-rich magma as indicated by the occurrence of carbonatites at some of the Cape Verde islands. F, Cl and Br were also detected in the two events, as well as As and Se, plus the heavy metals Tl and Pb (potentially hazardous to health), which are indicative of the composition of the volcanic gases.

Contrasting with the formation of compounds/minerals under strictly defined conditions in the laboratory, active volcanoes produce fumarole incrustations that are an indirect source of information of the harmful elements exhaled, as well as a mineralogical finger print of these complex dynamic systems.

References

522 Africano F, Bernard A (2000) Acid alteration in the fumarolic environment of Usu volcano,
523 Hokkaido, Japan. J Volcanol Geotherm Res 97:475-495. https://doi.org/10.1016/S0377-
524 0273(99)00162-6
525 Africano F, Van Rompaey G, Bernard A, Le Guern F (2002) Deposition of trace elements from
526 high temperature gases of Satsuma-Iwojima volcano. Earth Planet Sp 54:275-286.
527 https://doi.org/10.1186/BF03353027
528 Aiuppa A (2015) Volcanic-gas monitoring. In: Schmidt A, Fristad KE and Elkins-Tanton LT
529 (eds) Volcanism and Global Environmental Change, Cambridge University Press, 81-96.
530 https://doi.org/10.1017/CBO9781107415683.009
531 Allen AG, Oppenheimer C, Ferm M, Baxter PJ, Horrocks LA, Galle B, McGonigle AJS, Duffell
532 HJ (2002) Primary sulfate aerosol and associated emissions from Masaya Volcano,
533 Nicaragua. J Geophys Res 107:4682. doi: 10.1029/2002JD002120
534 Assunção CFT, Machado F, Gomes RA (1965) On the occurrence of carbonatites in the Cape
535 Verde Islands. Bol Soc Geol Port 16:179-188
536 Baker PE, Gass IG, Harris PG, Le Maitre RW (1964) The volcanological report of the Royal
537 Society expedition to Tristan da Cunha, 1962. Phil Trans Roy Soc London A256:439-575
538 Balić-Žunić T, Garavelli A, Jakobsson SP, Jonasson K, Katerinopoulos A, Kyriakopoulos K,
539 Acquafredda P (2016a) Fumarolic Minerals: An Overview of Active European Volcanoes.
540 In: Nemeth K (ed) Updates in Volcanology - From Volcano Modelling to Volcano Geology,
541 InTech Open Access Publishers, pp 267-322. doi: 10.5772/64129
542 Benedetto C, Forti P, Galli E, Rossi A (1998) Chemical deposits in volcanic caves of Argentina.
543 Int J Speleol 27B:155-162
544 Bobade SM, Gopalan P, Kulkarni AR (2009) Phase transition in Na_2SO_4: all five polymorphic
545 transformations in DSC. Ionics 15:353-355. doi: 10.1007/s11581-008-0272-6

546 Brodale GE, Giauque WE (1972) The relationship of crystalline forms I, III, IV, and V of
547 anhydrous sodium sulfate as determined by the third law of thermodynamics. J Phys Chem
548 76:737-743. doi: 10.1021/j100649a024
549 Carvalho MR, Mateus A, Nunes JC, Carvalho JM (2014) Origin and chemical nature of the
550 thermal fluids at Caldeiras da Ribeira Grande (Fogo Volcano, S. Miguel Island, Azores). In:
551 Sauer U and Dietrich P (Guest eds) Environ Earth Sci, Springer. doi: 10.1007/s12665-014-
552 3585-y
553 Chiodini G, Brombach T, Caliro S, Cardellini C (2002) Geochemical indicators of possible
554 ongoing volcanic unrest at Nisyros Island (Greece). Geophys Res Lett 29:6-1-6-4.
555 https://doi.org/10.1029/2001GL014355
556 Chiodini G, Cioni R, Marini L, Panichi C (1995) Origin of the fumarolic fluids of Vulcano
557 Island, Italy and implications for volcanic surveillance. Bull Volcanol 57:99-110.
558 https://doi.org/10.1007/BF00301400
559 Choi B-K, Lockwood DJ (2005) Peculiarities of the structural phase transitions in Na_2SO_4 (V): a
560 Raman scattering study. J Phys: Condens Matter 17:6095-6108. doi: 10.1088/0953-
561 8984/17/38/013
562 Cronin SJ, Neall VE, Lecointre JA, Hedley MJ, Loganathan P (2003) Environmental hazards of
563 fuoride in volcanic ash: a case study from Ruapehu volcano, New Zealand. J Volcanol
564 Geotherm Res 121:271-291. https://doi.org/10.1016/S0377-0273(02)00465-1
565 Day SJ, Heleno da Silva SIN, Fonseca JFBD (1999) A past giant lateral collapse and present-day
566 flank instability of Fogo, Cape Verde Islands. J Volcanol Geotherm Res 94:191–218.
567 https://doi.org/10.1016/S0377-0273(99)00103-1
568 Deer WA, Howie RA, Zussman J (1967) Gypsum. In: Rock-Forming Minerals, Non-silicates,
569 vol. 5, Longmans, London, 202-217

570 De Moor JM, Fischer TP, Sharp ZD, King PL, Wilke M, Botcharnikov RE, Cottrell E, Zelenski
571 M, Marty B, Klimm K, Rivard C, Ayalew D, Ramirez C, Kelley KA (2013) Sulfur
572 degassing at Erta Ale (Ethiopia) and Masaya (Nicaragua) volcanoes: Implications for
573 degassing processes and oxygen fugacities of basaltic systems. Geochem Geophys Geosyst
574 14:4076-4108. https://doi.org/10.1002/ggge.20255
575 Dionis SM, Melián G, Rodríguez F, Hernández PA, Padrón E, Pérez NM, Barrancos J, Padilla G,
576 Sumino H, Fernandes P, Bandomo Z, Silva S, Pereira JM, Semedo H (2015a) Diffuse
577 volcanic gas emission and thermal energy release from the summit crater of Pico do Fogo,
578 Cape Verde. Bull Volcanol 77:10. doi: 10.1007/s00445-014-0897-4
579 Dionis SM, Pérez NM, Hernández PA, Melián G, Rodríguez F, Padrón E, Sumino H, Barrrancos
580 J, Padilla GD, Fernandes P, Bandomo Z, Silva S, Pereira JM, Semedo H, Cabral J (2015b)
581 Diffuse CO_2 degassing and volcanic activity at Cape Verde islands, West Africa. Earth,
582 Planets Space 67:48. doi 10.1186/s40623-015-0219-x
583 Doucelance R, Hammouda T, Moreira M, Martins JC (2010) Geochemical constraints on depth
584 of origin of oceanic carbonatites: The Cape Verde case. Geochim Cosmochim Acta
585 74:7261-7282. doi:10.1016/j.gca.2010.09.024
586 Ellis DR, Salt DE (2003) Plants, selenium and human health. Curr Opin Plant Biol 6:273-279.
587 https://doi.org/10.1016/S1369-5266(03)00030-X
588 Eysel W, Höfer HH, Keester KL, Hahn Th (1985) Crystal chemistry and structure of Na_2SO_4 (I)
589 and its solid solutions. Acta Cryst B41:5-11
590 Fang JH, Robinson PD (1972) Crystal Structures and Mineral Chemistry of Double-Salt
591 Hydrates: II. The Crystal Structure of Mendozite, $NaAl(SO_4)_2.11H_2O$. Am Min 57:1081-
592 1088

593 Ferrara G, Garavelli A, Pinarelli L, Vurro F (1995) Lead isotope composition of the sublimates
594 from the fumaroles of Vulcano (Aeolian Islands, Italy): inferences on the deep fluid
595 circulation. Bull Volcanol 56:621-625. https://doi.org/10.1007/BF00301466
596 Figueiredo E, Fonte J, Lima A, Veiga JP, Silva RJC, Mirão J (2018) Ancient tin production:
597 Slags from the Iron Age Carvalhelhos hillfort (NW Iberian Peninsula). J Archaeol Sci 93: 1-
598 16. https://doi.org/10.1016/j.jas.2018.02.007
599 Figueiredo MO (1997) Orange gel masses associated with the eruption of 1995 on Fogo Island: a
600 new mineral? (in Portuguese). In: Réffega A et al. (eds) A erupção vulcânica de 1995 na ilha
601 do Fogo, Cabo Verde, IICT, Lisbon, Portugal, pp 201-210
602 Figueiredo MO, Silva LC, Pereira da Silva T, Torres PC, Mendes MH (1997) Mineralogy of the
603 incrustations resulting from the fumarole activity from the 1995 eruption of the Fogo island,
604 Cape Verde (in Portuguese). In: Réffega A et al. (eds) A erupção vulcânica de 1995 na ilha
605 do Fogo, Cabo Verde, IICT, Lisbon, Portugal, pp 187-199
606 Figueiredo MO, Silva TP, Basto MJ, Ramos MT, Chevallier P (1999) Indirect monitoring of
607 heavy metals in volcanic gases by synchrotron X-ray microprobe (μ-SRXRF) qualitative
608 analysis of sublimates. J Anal At Spectrom 14:505-507. doi: 10.1039/A808103D
609 Fischer TP (2008) Fluxes of volatiles (H_2O, CO_2, N_2, Cl, F) from arc volcanoes. Geochem J
610 42:21-38. https://doi.org/10.2343/geochemj.42.21
611 Flörke OW (1952) Kristallographische und röntgenographische Untersuchungen im System,
612 $CaSO_4$-$CaSO_4.2H_2O$. Neues Jahrb Min, Abh 84:189-240
613 Giggenbach WF (1996) Chemical Composition of Volcanic Gases. In: Scarpa R and Tilling RI
614 (eds) Monitoring and Mitigation of Volcano Hazards, Springer, Berlin, 221-256. doi:
615 10.1007/978-3-642-80087-0_7
616 Global Volcanism Program (2017) Report on Fogo (Cape Verde). In: Venzke E (ed), Bulletin of
617 the Global Volcanism Network 42:9. Smithsonian Institution

618 Hardie LA (1967) The gypsum-anhydrite equilibrium at one atmosphere pressure. Am Miner
619 52:171-200
620 Hernández PA, Melián GV, Dionis S, Barrancos J, Padilla G, Padrón E, Silva S, Fernandes P,
621 Cardoso N, Pérez NM, Rodríguez F, Asensio-Ramos M, Calvo D, Semedo H, Alfama V
622 (2015) Chemical composition of volcanic gases emitted during the 2014-15 Fogo eruption,
623 Cape Verde. Geophys Res Abst 17:EGU2015-9577
624 Jakobsson SP, Leonardsen ES, Balic-Zunic T, Jónsson SS (2008) Encrustations from three recent
625 volcanic eruptions in Iceland: the 1963-1967 Surtsey, the 1973 Eldfelland and the 1991
626 Hekla eruptions. Fjölrit Náttúrufræðistofnunar 52: 65 pp
627 Jenkins SF, Day SJ, Faria BE, Fonseca JFBD (2017) Damage from lava flows: insights from the
628 2014-2015 eruption of Fogo, Cape Verde. J Appl Volcanol 6:6. doi: 10.1186/s13617-017-
629 0057-6
630 Kishimura H, Imasu Y, Matsumoto H (2015) Thermal dehydration of potash alum studied by
631 Raman spectroscopy and X-ray diffraction analysis. Mat Chem Phys 149-150:99-104.
632 http://dx.doi.org/10.1016/j.matchemphys.2014.09.049
633 Kodosky L, Keskinen M (1990) Fumarole distribution, morphology, and encrustation
634 mineralogy associated with the 1986 eruptive deposits of mount St. Augustine, Alaska. Bull
635 Volcanol 52:175-185. https://doi.org/10.1007/BF00334803
636 Kracek, FC (1929) The polymorphism of sodium sulphate. I: Thermal analysis. J Phys Chem
637 33:1281-1303. doi: 10.1021/j150303a001
638 Lacroix A (1907) Les mineraux des fumerolles de l'eruption du Vesuve en avril 1906. Bull Soc
639 Min Fr 30 :219-226
640 Le Guern F, Bernard A (1982) Etude des mecanismes de condensation des gaz magmatiques -
641 exemple de l'Etna (Italie). Bull Volcanol 45:161-166. https://doi.org/10.1007/BF02597725

642 Lenz M, Lens PNL (2009) The essential toxin: the changing perception of selenium in
643 environmental sciences. Sci Total Environ 407:3620-3633. doi:
644 10.1016/j.scitotenv.2008.07.056
645 Linnow K, Zeunert A, Steiger M (2006) Investigation of Sodium Sulfate Phase Transitions in a
646 Porous Material Using Humidity- and Temperature-Controlled X-ray Diffraction. Anal
647 Chem 78: 4683-4689. doi: 10.1021/ac0603936
648 Lombardi G, Sposato A (1981) Tamarugite from Vulcano, Aeolian Islands, Italy. Can Mineral
649 19:403-407
650 Maccaferri F, Richter N, Walter TR (2017) The effect of giant lateral collapses on magma
651 pathways and the location of volcanism. Nat Commun 8:1097. doi: 10.1038/s41467-017-
652 01256-2
653 Mackenzie KM, Rodgers KA, Browne PRL (1995) Tamarugire, $NaAl(SO_4)_2.6H_2O$, from Te
654 Kopia, New Zealand. Min Mag 59:754-757
655 Martin RS, Sawyer GM, Spampinato L, Salerno GG, Ramirez C, Ilyinskaya E, Witt MLI,
656 Mather TA, Watson IM, Phillips JC, Oppenheimer C (2010) A total volatile inventory for
657 Masaya Volcano, Nicaragua. J Geophys Res 115:B09215. doi: 10.1029/2010JB007480
658 Martins S, Mata J, Munhá J, Mendes MH, Maerschalk C, Caldeira R, Mattielli N (2010)
659 Chemical and mineralogical evidence of the occurrence of mantle metasomatism by
660 carbonate-rich melts in an oceanic environment (Santiago Island, Cape Verde). Miner Petrol
661 99:43-65. https://doi.org/10.1007/s00710-009-0078-x
662 Mata J, Martins S, Mattielli N, Madeira J, Faria B, Ramalho RS, Silva P, Moreira M, Caldeira R,
663 Moreira M, Rodrigues J, Martins L (2017) The 2014-15 eruption and the short-term
664 geochemical evolution of the Fogo volcano (Cape Verde): Evidence for small-scale mantle
665 heterogeneity. Lithos 288-289:91-107. doi: 10.1016/j.lithos.2017.07.001

Mehrotra BN, Hahn, Th, Arnold H, Eysel W (1975) Polymorphism of Na_2SO_4. Acta Crystallogr A31, Supplement:S79

Melián G, Tassi F, Pérez N, Hernández P, Sortino F, Vaselli O, Padrón E, Nolasco D, Barrancos J, Padilla G, Rodríguez F, Dionis S, Calvo D, Notsu K, Sumino H (2012) A magmatic source for fumaroles and diffuse degassing from the summit crater of Teide Volcano (Tenerife, Canary Islands): a geochemical evidence for the 2004–2005 seismic–volcanic crisis. Bull Volcanol 74:1465-1483. https://doi.org/10.1007/s00445-012-0613-1

Naughton JJ, Greenberg VA, Goguel R (1976) Incrustations and fumarolic condensates at Kilauea volcano, Hawaii: field, drill-hole and laboratory observations. J Volcanol Geotherm Res 1:149-165. https://doi.org/10.1016/0377-0273(76)90004-4

Orlando V, Franco T, Dario T, Robert PJ, Antonio C (2011) Submarine and inland gas discharges from the Campi Flegrei (southern Italy) and the Pozzuoli Bay: geochemical clues for a common hydrothermal-magmatic source. Procedia Earth Planet Sci 4:57-73. doi:10.1016/j.proeps.2011.11.007

Óskarsson N (1981) The chemistry of icelandic lava incrustations and the latest stages of degassing. J Volcanol Geotherm Res 10:93-111. https://doi.org/10.1016/0377-0273(81)90057-3

Óskarsson N (1984) Monitoring of fumarole discharge during the 1975–1982 rifting in Krafla volcanic center, north Iceland. J Volcanol Geotherm Res 22:97-121. https://doi.org/10.1016/0377-0273(84)90036-2

Palache C, Berman H, Frondel C (1951) The system of mineralogy. John Wiley and Sons, Inc., London

Paonita A, Federico C, Bonfanti P, Capasso G, Inguaggiato S, Italiano F, Madonia P, Pecoraino G, Sortino F (2013) The episodic and abrupt geochemical changes at La Fossa fumaroles (Vulcano Island, Italy) and related constraints on the dynamics, structure, and compositions

691 of the magmatic system. Geochim Cosmochim Acta 120:158-178.
692 http://dx.doi.org/10.1016/j.gca.2013.06.015
693 Pekov IV, Gurzhiy VV, Zubkova, NV, Agakhanov AA, Belakovskiy DI, Vigasina MF, Sidorov,
694 EG (2016) Metathénardite, IMA 2015-102. CNMNC Newsletter No. 30, April 2016, page
695 408; Min Mag 80:407-413. doi: 10.1180/minmag.2016.080.081
696 Pekov IV, Zubkova NV, Yapaskurt VO, Belakovskiy DI, Lykova IS, Vigasina MF, Sidorov EG,
697 Pushcharovsky DYu (2014) New arsenate minerals from the Arsenatnaya fumarole,
698 Tolbachik volcano, Kamchatka, Russia. I. Yurmarinite, $Na_7(Fe^{3+},Mg,Cu)_4(AsO_4)_6$. Min Mag
699 78:905-917. doi: 10.1180/minmag.2014.078.4.10
700 Pelloux A (1927) The minerals of Vesuvius. Am Miner 12:14-21
701 Prasad PSR, Ravikumar N, Krishnamurthy ASR, Sarma LP (1998) Role of impurities in
702 gypsum-bassanite phase transition: A comparative Raman study. Curr Sci 75:1410-1414
703 Quisefit JP, Toutain JP, Bergametti G, Javoy M, Cheynet B, Person A (1989) Evolution versus
704 cooling of gaseous volcanic emissions from Momotombo Volcano, Nicaragua:
705 Thermochemical model and observations. Geochim Cosmochim Acta 53:2591-2608.
706 https://doi.org/10.1016/0016-7037(89)90131-2
707 Rasmussem SE, Jørgensen J-E, Lundtoft B (1996) Structures and phase transitions of Na_2SO_4. J
708 Appl Cryst 29:42-47. https://doi.org/10.1107/S0021889895008818
709 Ribeiro O (1998) The Fogo Island and its eruptions (in Portuguese). Comissão Nacional para as
710 Comemorações dos Descobrimentos Portugueses, Lisbon
711 Richter N, Favalli M, Dalfsen EZ, Fornaciai A, Fernandes RMS, Pérez NM, Levy J, Victória SS,
712 Walter TR (2016) Lava flow hazard at Fogo Volcano, Cabo Verde, before and after the
713 2014-2015 eruption. Nat Hazards Earth Syst Sci 16:1925-1951. doi:10.5194/nhess-16-1925-
714 2016

715 Rodríguez-Mercado JJ, Altamirano-Lozano M (2013) Genetic toxicology of thallium: a review.
716 Drug Chem Toxicol 36:369-383. doi: 10.3109/01480545.2012.710633
717 Rodriguez-Navarro C, Doehnea E, Sebastian E (2000) How does sodium sulfate crystallize?
718 Implications for the decay and testing of building materials. Cem Concr Res 30:1527-1534
719 Rose WI (1973) Pattern and mechanism of volcanic activity at the Santiaguito Volcanic Dome,
720 Guatemala. Bull Volcanol 37:73-94. https://doi.org/10.1007/BF02596881
721 Rosenberg PE (1988) Aluminum fluoride hydrates, volcanogenic salts from Mount Erebus,
722 Antarctica. Am Miner 73:855-860
723 Schaller T, Dingwell DB, Keppler H, Knöller W, Merwin L, Sebald A (1992) Fluorine in silicate
724 glasses: A multinuclear nuclear magnetic resonance study. Geochim Cosmochim Acta
725 56:701-707. doi: 10.1016/0016-7037(92)90091-V
726 Shinohara H (2013) Volatile flux from subduction zone volcanoes: Insights from a detailed
727 evaluation of the fluxes from volcanoes in Japan. J Volcanol Geotherm Res 268:46-63.
728 https://doi.org/10.1016/j.jvolgeores.2013.10.007
729 Silva LC, Le Bas MJ, Robertson AHF (1981) An oceanic carbonatite volcano on Santiago, Cape
730 Verde Islands. Nature 294:644-645. https://doi.org/10.1038/294644a0
731 Silva LC, Mendes MH, Torres PC, Palácios T, Munhá JM (1997) Petrography and mineralogy of
732 the volcanic formations from the 1995 eruption of the Fogo island, Cape Verde (in
733 Portuguese). In: Réffega A et al. (eds) A erupção vulcânica de 1995 na ilha do Fogo, Cabo
734 Verde, IICT, Lisbon, Portugal, pp 165-170
735 Silva TP (1999) Minerochemistry of incrustations and fumarole sublimates from Fogo island
736 volcano (Cape Verde) (in Portuguese). Dissertation equivalent to PhD, IICT-Instituto de
737 Investigação Científica Tropical (ed), Lisbon, Portugal, 159 pp.
738 Silva TP, de Oliveira D, Veiga JP, Ávila P, Candeias C, Salas-Colera E, Caldeira R (2018)
739 Selenium retained by minerals from volcanic fumaroles at Fogo island (Cape Verde). In:

740 Oliveira A et al. (eds) Abstracts book of XIV Congresso de Geoquímica dos Países de
741 Língua Portuguesa, UTAD, Portugal, pp 511-514
742 Solé VA, Papillon E, Cotte M, Walter Ph, Susini J (2007) A multiplatform code for the analysis
743 of energy-dispersive X-ray fluorescence spectra. Spectrochim Acta 62:63-68. doi:
744 10.1016/j.sab.2006.12.002
745 Steiger M, Asmussen S (2008) Crystallization of sodium sulfate phases in porous materials: The
746 phase diagram Na_2SO_4–H_2O and the generation of stress. Geochim Cosmochim Acta
747 72:4291-4306. doi:10.1016/j.gca.2008.05.053
748 Stoiber RE, Rose WI (1969) Recent volcanic and fumarolic activity at Santiaguito Volcano,
749 Guatemala. Bull Volcanol 33:475-502. doi: 10.1007/BF02596520
750 Stoiber RE, Rose WI (1970) The Geochemistry of Central American Volcanic Gas Condensates.
751 GSA Bulletin 81:2891-2912. https://doi.org/10.1130/0016-
752 7606(1970)81[2891:TGOCAV]2.0.CO;2
753 Stoiber RE, Rose WI (1974) Fumarole incrustations at active Central American volcanoes.
754 Geochim Cosmochim Acta 38:495-516. https://doi.org/10.1016/0016-7037(74)90037-4
755 Symonds RB, Reed MH, Rose WI (1992) Origin, speciation, and fluxes of trace-element gases at
756 Augustine volcano, Alaska: Insights into magma degassing and fumarolic processes.
757 Geochim Cosmochim Acta 56:633:657. https://doi.org/10.1016/0016-7037(92)90087-Y
758 Symonds RB, Rose WI, Bluth GJS, Gerlach TM (1994) Volcanic gas studies: methods, results,
759 and applications. In: Carroll MR and Holloway JR (eds) Volatiles in Magmas. Reviews in
760 Mineralogy 30: 1-66. http://www.minsocam.org/MSA/RIM/Rim30.html
761 Symonds RB, Rose WI, Reed MH, Lichte FE, Finnegan DL (1987) Volatilization, transport and
762 sublimation of metallic and non-metallic elements in high temperature gases at Merapi
763 Volcano, Indonesia. Geochim Cosmochim Acta 51:2083-2101. doi: 10.1016/0016-
764 7037(87)90258-4

765 Taide ST, Ingle NB, Omanwar SK (2015) Characterization and photoluminescence studies of
766 Dy^{3+} doped Na_2SO_4 phosphor prepared by re-crystallization method. IOSR J Appl Phys
767 7:27-32. doi: 10.9790/4861-07312732
768 Taran Y, Zelenski M (2015) Systematics of water isotopic composition and chlorine content in
769 arc-volcanic gases. Geological Society, London, Special Publications 410(1):237-262.
770 http://dx.doi.org/10.1144/SP410.5
771 Tchounwou PB, Yedjou CG, Patlolla AK, Sutton DJ (2012) Heavy Metal Toxicity and the
772 Environment. In: Luch A (ed) Molecular, Clinical and Environmental Toxicology. Exp
773 Suppl 101:133-164, Springer, Basel. doi: 10.1007/978-3-7643-8340-4_6
774 Torres PC, Madeira J, Silva LC, Silveira AB, Serralheiro A, Mota Gomes, A (1997) Geologic
775 map of the historical eruptions of Fogo Island: review and update (in Portuguese). In:
776 Réffega A et al. (eds) A erupção vulcânica de 1995 na ilha do Fogo, Cabo Verde, IICT,
777 Lisbon, Portugal, pp 119-132
778 Torres PC, Silva LC, Mota Gomes A (1995) Geology and volcanology of the 1995 eruption on
779 the Fogo island-Cape Verde archipelago (in Portuguese). In: Porto University (ed)
780 Memórias do Museu e Laboratório Mineralógico e Geológico da Faculdade de Ciências da
781 Universidade do Porto, pp 1019-1023
782 Toutain JP, Aloupogiannis P, Delorme H, Person A, Blanc P, Robaye G (1990) Vapor
783 deposition of trace elements from degassed basaltic lava, Piton de la Fournaise volcano,
784 Reunion Island. J Volcanol Geotherm Res 40:257-268. https://doi.org/10.1016/0377-
785 0273(90)90124-X
786 Vergasova LP, Filatov, SK (2016) A Study of Volcanogenic Exhalation Mineralization. J
787 Volcanol Seismol 10:71-85. doi: 10.1134/S0742046316020068

788 Vidya YS, Lakshminarasappa BN (2013) Preparation, Characterization, and Luminescence
789 Properties of Orthorhombic Sodium Sulphate. Phys Res Int 2013:Article ID 641631, 7
790 pages. https://doi.org/10.1155/2013/641631
791 Vieira G, Pina P, Mora C, Fernandes R, Almeida P, Dumont S, Martins B, Candeias C, Oliveira
792 C, Ramalho RS (2017) Very high-resolution aerophotogrametric survey of the 2014/2015
793 lava flow field of Fogo volcano (Cape Verde). Proceedings of the 5th International
794 Conference on "Small Unmanned Aerial Systems for Environmental Research", Vila Real,
795 Portugal, pp 49-50
796 Wahrenberger C, Seward TM, Dietrich V (2002) Volatile trace-element transport in high-
797 temperature gases from Kudriavy volcano (Iturup, Kurile Islands, Russia). In: Hellmann R
798 and Wood SA (eds) Water-Rock Interactions, Ore Deposits, and Environmental
799 Geochemistry: A Tribute to David A. Crerar, Geochem Soc Spec Publ 7: 307-327.
800 https://ci.nii.ac.jp/naid/10018296233
801 Williams SN, Self S (1983) The October 1902 Plinian eruption of Santa Maria Volcano,
802 Guatemala. J Volcanol Geotherm Res 16:33–56. https://doi.org/10.1016/0377-
803 0273(83)90083-5
804 Wu D, Sun S (2016) Speciation analysis of As, Sb and Se. Trends Env Anal Chem 11:9-22.
805 https://doi.org/10.1016/j.teac.2016.05.001
806 Zelenski M, Taran Y (2011) Geochemistry of volcanic and hydrothermal gases of Mutnovsky
807 volcano, Kamchatka: evidence for mantle, slab and atmosphere contributions to fluids of a
808 typical arc volcano. Bull Volcanol 73: 373-394. https://doi.org/10.1007/s00445-011-0449-0
809
810
811
812

Figure Captions

Fig. 1 a Map of the Cape Verde Archipelago. Satellite images of Fogo Island: **b** From Sentinel 2 captured on 6 February 2017 (true colour RGB composite); **c** Sampling sites, adapted from Global Volcanism Program, 2017 (image captured on 24 December 2014)

Fig. 2 Younger Pico do Fogo volcano (principal eruptive cone) is the highest point on Fogo Island (Cape Verde) inside the Chã das Caldeiras (around 1100 m high): **a** view of the steep rock wall (Bordeira) that reaches 1 km in height; **b** location of the last two eruptive events (the 2014-15 eruption occurred on the flank of the previously formed 1995 cinder cone), viewed at a distance of about 1500 m across the Chã das Caldeiras

Fig. 3 Main vent of 2014-15 eruption on Fogo Island (distance around 3 km between main vent and Bordeira) and lava flow field at Chã das Caldeiras

Fig. 4 Samples of rocks (basaltic lava) and incrustations collected in November 2016, from near the 2014-15 main vent (see Table 1 for description)

Fig. 5 February 2017 sampling campaign: **a** Sulphur (F9, yellow) close to the main vent and the registered temperature near the sample. **b** Unstable fracture where white incrustations (F18, 182°C) were collected along the walls. **c** The highest temperature (238°C) was measured at the bottom of a pit lined containing white material (F19)

836 **Fig. 6** Image of the smaller vent, called “vulcãozinho” (little volcano) by the local population,
837 located at a lower altitude than the principal vent. The circle marks a person for scale near the
838 main vent
839
840 **Fig. 7** White incrustations (F24) surrounding “vulcãozinho”. View of a pit with a big tunnel
841 crossing it, also containing white material
842
843 **Fig. 8** Stereomicroscope images of some studied samples with the corresponding mineralogical
844 phases assigned: F8-white crystals (A-Anhydrite+Ba-Bassanite); F8-whitish hyaline material (G-
845 Gypsum+A-Anhydrite); F19-white material (H-Halite+T-Thenardite+SS-Sodium sulphate, form
846 III)
847
848 **Fig. 9** XRD pattern collected from white material of sample F19/17. Assigned phases in
849 decreasing percentage: H, halite (NaCl); T, thenardite (Na_2SO_4); SS (sodium sulphate, form III)
850
851 **Fig. 10** Energy dispersive X-ray fluorescence (EDXRF) spectra (excitation energy of 29.58 keV)
852 collected for samples F9/17 (sulphur aggregate), F19/17 (white material), F20/17A and D (white
853 material aggregate and disaggregate, respectively). Only the diagnostic line of each element is
854 assigned
855

Figure 1

Click here to access/download;Figure;Fig 1.tif

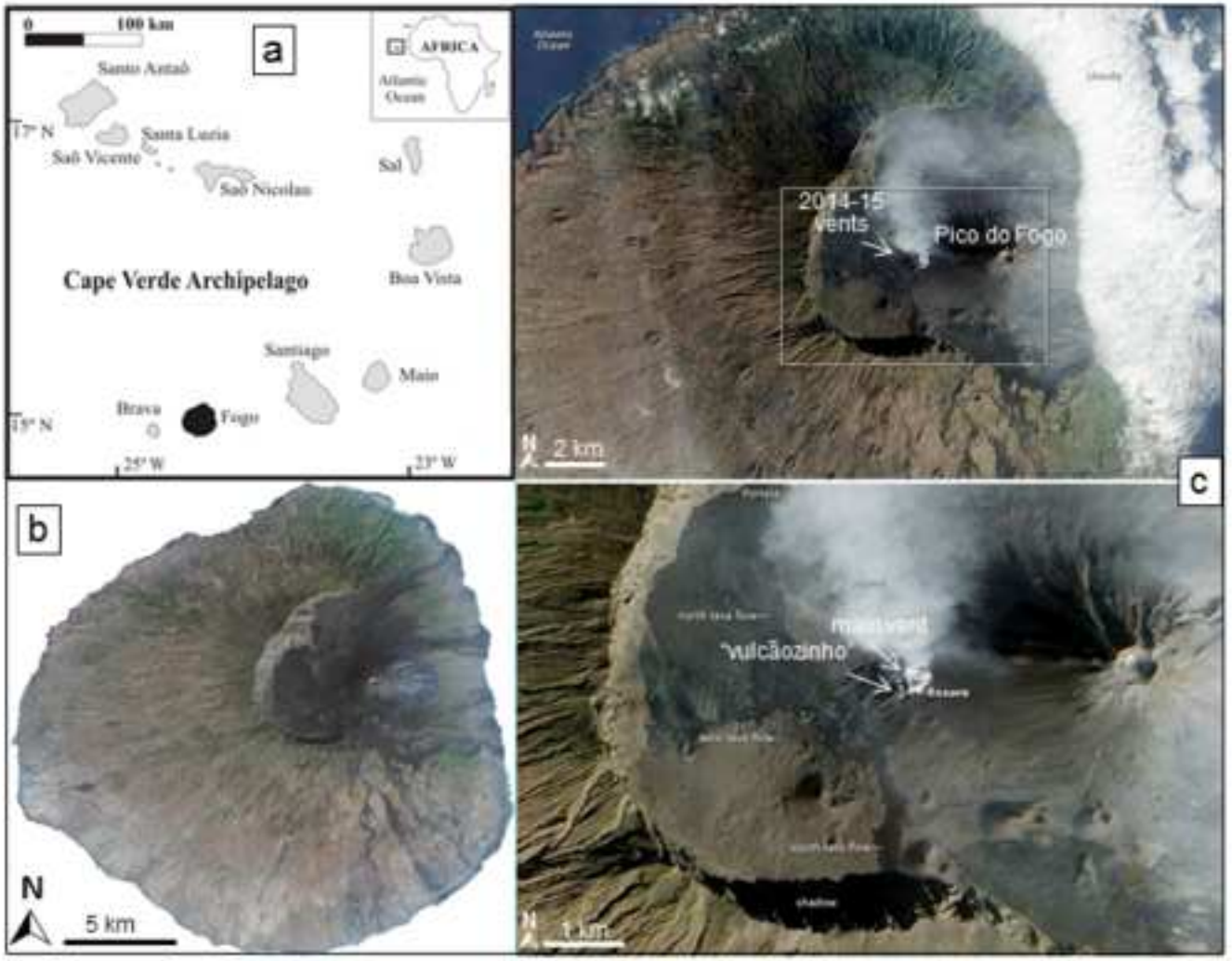

Figure 2

Click here to access/download;Figure;Fig 2.tif

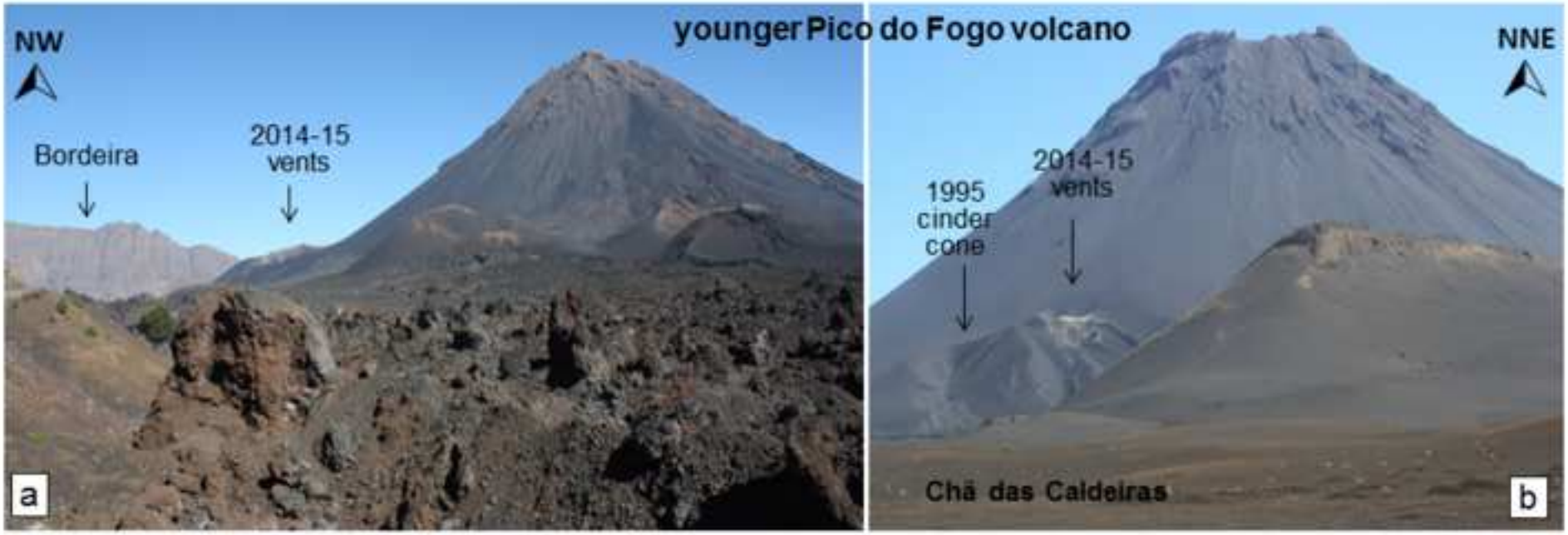

Figure 3

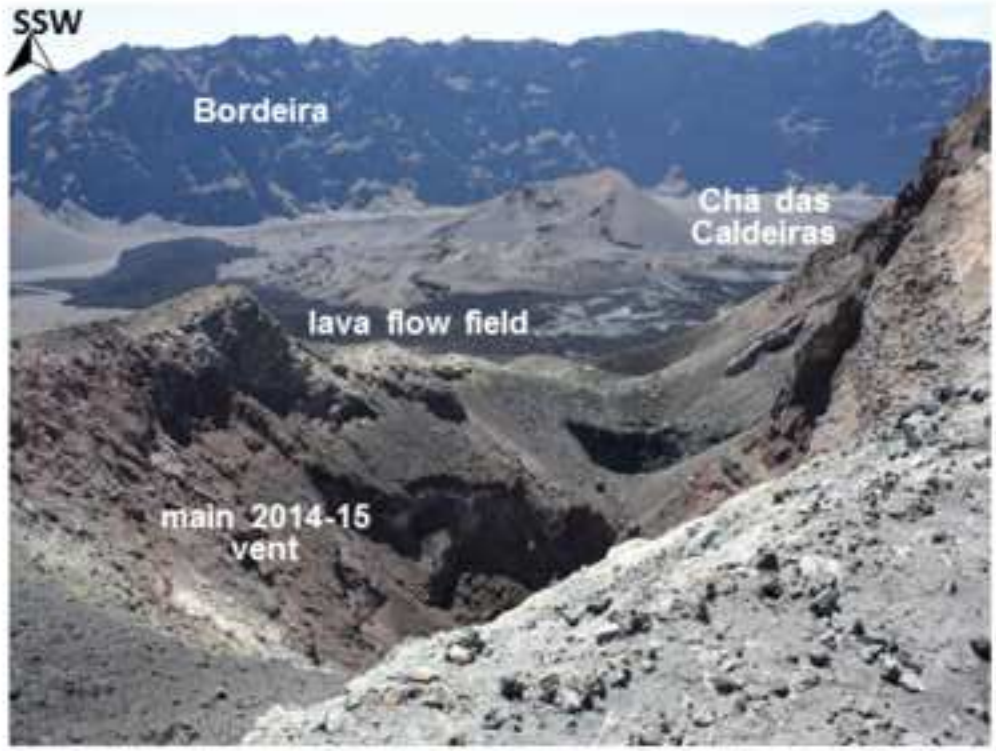

Figure 4

Click here to access/download;Figure;Fig 4.tif

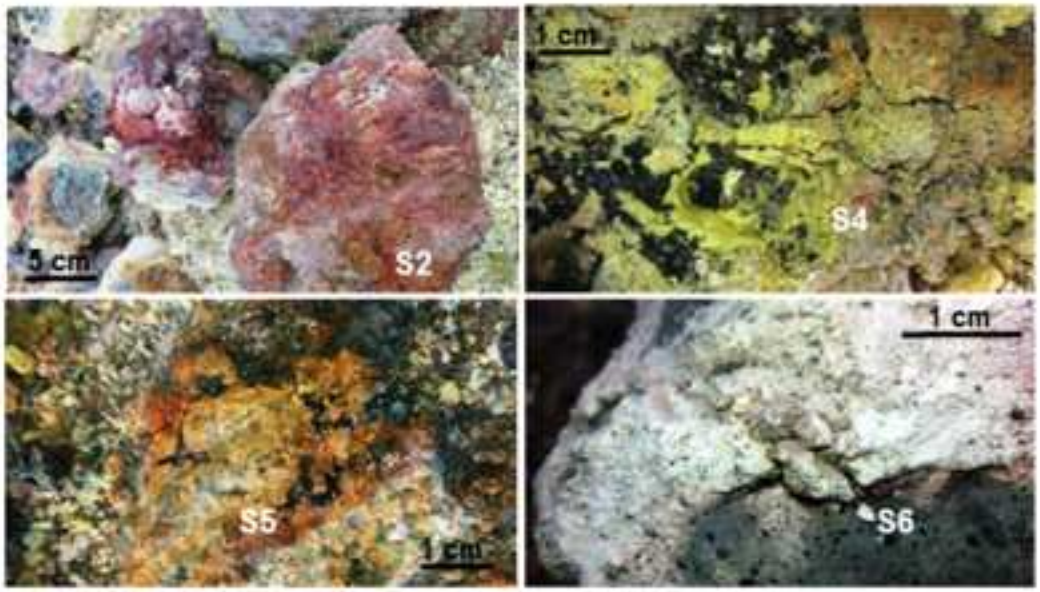

Figure 5

Click here to access/download;Figure;Fig 5.tif

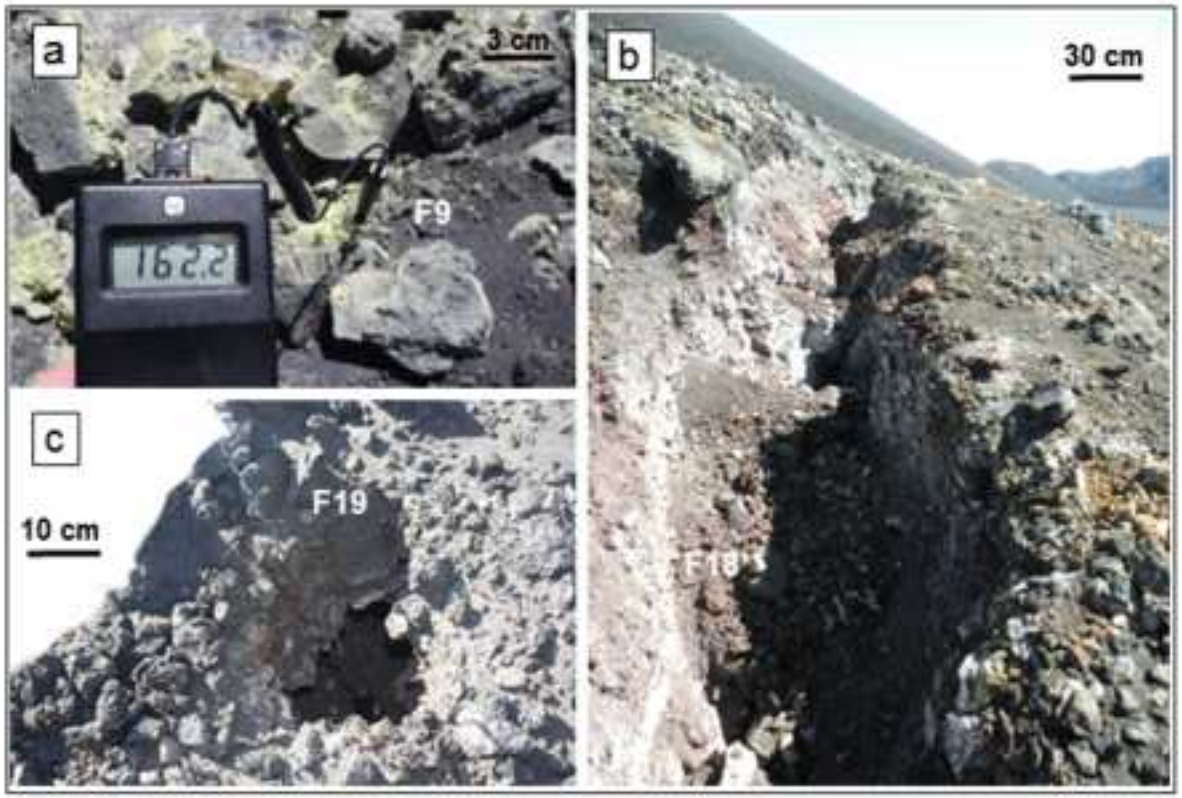

Figure 6

Click here to access/download;Figure;Fig 6.tif

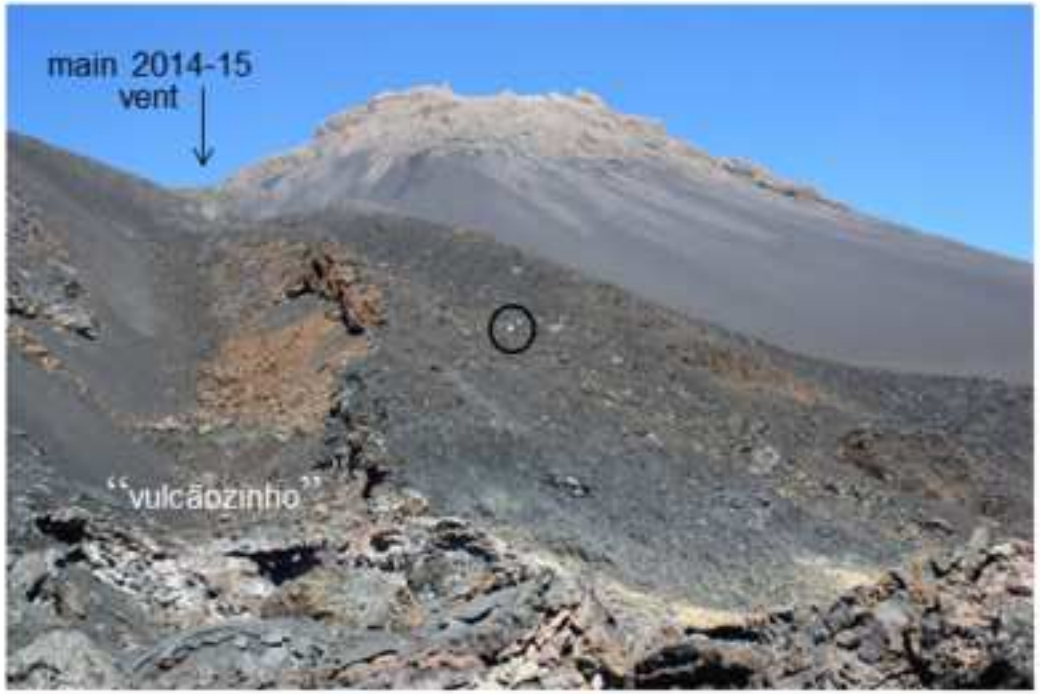

Figure 7

Figure 8

Click here to access/download;Figure;Fig 8.tif

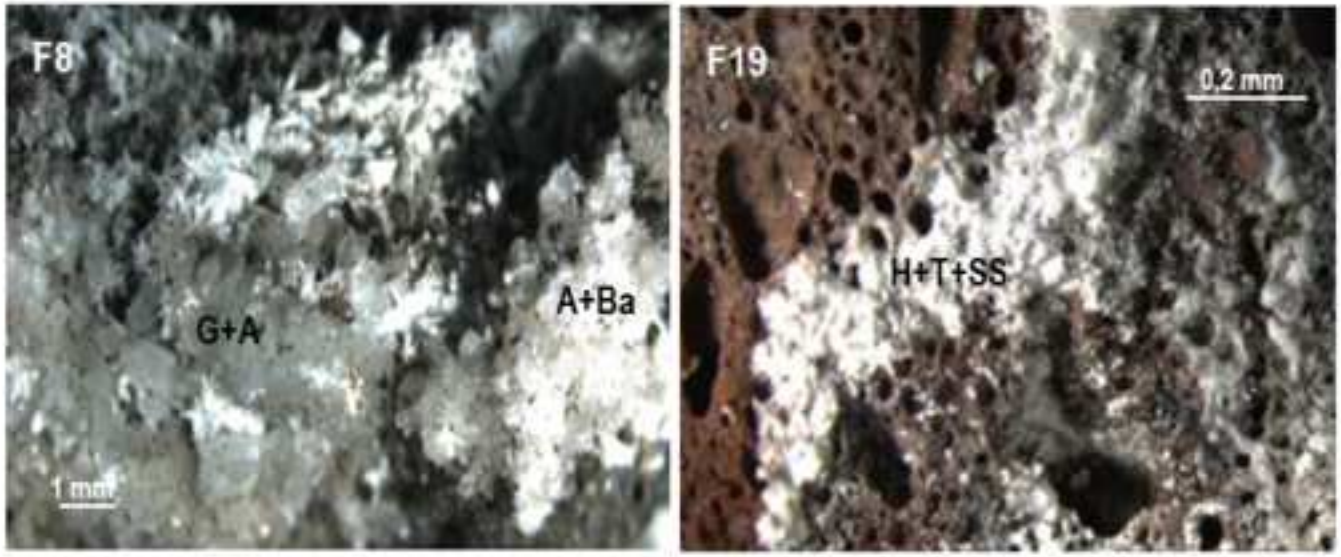

Figure 9

Click here to access/download;Figure;Fig 9.tif

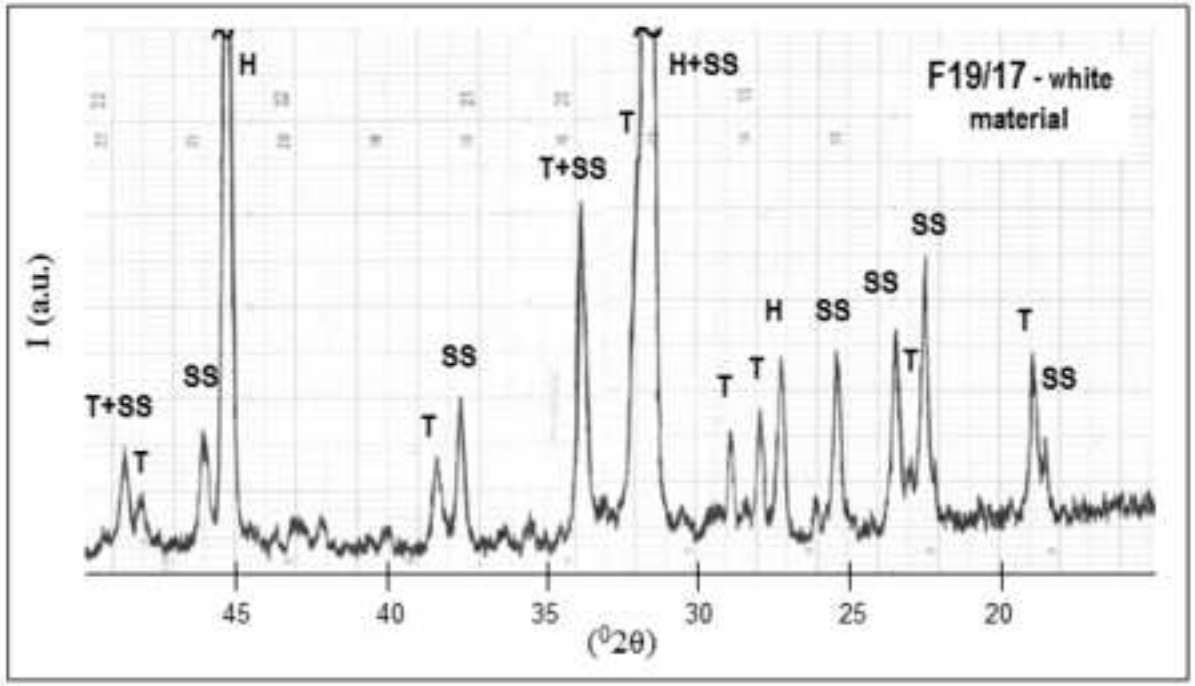

Figure 10

Click here to access/download;Figure;Fig 10.tif

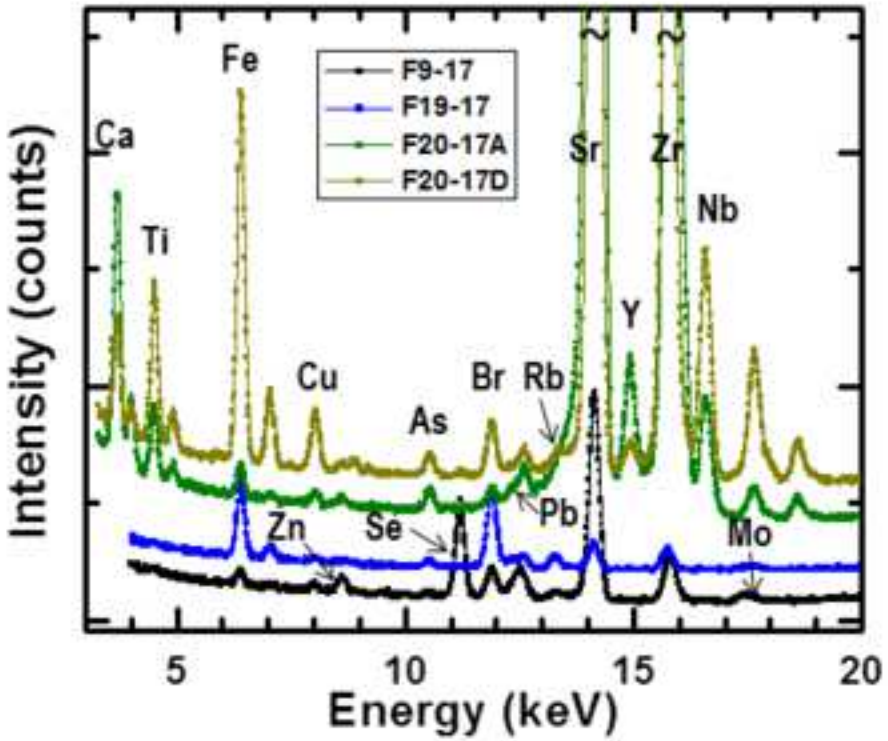

Table 1 Brief description of samples collected during two campaigns on Fogo volcano and measured temperature close to the sample

Sampling Campaign	Location	Sample reference	Description	Temperature (°C)
November 2016	Surroundings of the main vent (rocks with coloured incrustations deposited on the field)	S2	Reddish rock with white opaque crystals	
		S3	Rock with hyaline sulphur	
		S4	Aggregate with yellow and orange sulphur plus white incrustations	
		S5	Reddish/brownish rock with white opaque incrustations	
		S6	Whitish rock and pink	
February 2017		F8/17	Rock with hyaline sulphur, white crystals and whitish hyaline powder	
		F9/17	Sulphur aggregates and white incrustations	162
		F10/17	Reddish incrustation in the rock	
		F11/17	Rock with sulphur (aggregate and hyaline) and white incrustations	
		F12/17	White and yellow powders in the rock	
		F13/17	Greenish sulphur	
		F14/17	Reddish rock with white incrustations	
		F17/17	White aggregate on the field	76
		F25/17	White (hygroscopic) and yellowish incrustations	
		F26/17	White powder (dry)	
		F27/17	Yellow and brown-orange incrustations	
	Walls of an unstable fracture, near the main vent	F18/17	White powder	182
	Walls of a pit, near the main vent	F19/17	White powder	238
	"Vulcãozinho" (smaller vent)	F24/17	White powder	

Table 2

Table 2 XRD mineralogical characterization of incrustations from 2014-15 eruption of Fogo volcano, Cape Verde (JCPDF card quoted bellow)

Location	Sample reference	Description	Main identified phases
Main vent (field)	S2	Reddish rock	Amorphous
	S3	Rock with hyaline sulphur	S + Pi
	S4	Yellow sulphur	S
		Orange sulphur	S
		White incrustation and sulphur	A + S + G
	S5	Reddish rock with white opaque crystals	Pi + A
		Brownish rock with white powder	Pi + G
	S6	White and pink rock fragments	Amorphous + Pi
	F8/17	White crystals	A + Ba
		Whitish hyaline powder	G + A
	F9/17	Sulphur aggregate	S
		White incrustations	Ta + B
	F10/17	Reddish incrustation	A + Ba + S
	F11/17	Sulphur aggregate	S
		Hyaline sulphur	S
		White powder	A + Ba + S (vtg)
		White aggregate	Ba + A (vtg) + Pi? (vtg)
	F12/17	Powder scraped from the rock	Amorphous + G + A + S (vtg)
		Gypsum crystals?	G + A
		Sulphur aggregate	S + G (vtg)
		Hyaline sulphur	S + G (vtg)
	F13/17	Greenish sulphur	S + O (vtg)
	F14/17	Reddish rock	Ti + R
		White incrustations	Bl + T + P + H + S (vtg)
	F17/17	White aggregate	Ta + B
	F25/17	White incrustations (hygroscopic)	T + Bl + H?
		Yellowish incrustations	T + Bl + P + H + S (vtg)
	F26/17	White powder (dry)	T + Bl + H + P + S (vtg)
	F27/17	Yellow incrustations	Ti + R (vtg)
		Brown-orange incrustations	R
Main vent (fracture)	F18/17	White powder	A + Ba + S (vtg)
		Sub-rounded white crystals	Ba + A + G? (vtg)
		White opaque crystals	Amorphous + Ti?
Main vent (pit)	F19/17	White powder	H + T + SS
"Vulcãozinho" (smaller vent)	F24/17	White powder	T + H
Unknown	F20/17	White aggregate	A + G
		White powder (disaggregate)	G + A + S (vtg)

A - Anhydrite, $CaSO_4$ (#37-1496); **B** - Bianchite, $(Zn_{0.69}Fe_{0.21}Mg_{0.10})SO_4.6H_2O$ (#12-16); **Ba** - Calcium sulphate hydrate (Bassanite), $Ca_2(SO_4)_2.H_2O$ (#41-224); **Bl** - Bloedite, $Na_2Mg(SO_4)_2.4H_2O$ (#88-1789); **G** - Gypsum, $CaSO_4.2H_2O$ (#6-0046); **H** - Halite, NaCl (#5-0628); **O** - Olivine - Fayalite, Fe_2SiO_4 (#20-1139); **P** - Picromerite, $K_2Mg(SO_4)_2.6H_2O$ (#21-1400); **Pi** - Pyroxene - Diopside, $CaMg(SiO_3)_2$ (#71-1067); **R** – Ralstonite, $Na_{0.88}Mg_{0.88}Al_{1.12}(F,OH)_6.H_2O$ (#18-1085); **S** - Sulphur, S orthorhombic (#8-247); **SS** - Sodium sulphate (Form III), Na_2SO_4 (#24-1132); **T** - Thenardite, Na_2SO_4 (#37-1465); **Ta** - Tamarugite, $NaAl(SO_4)_2.6H_2O$ (#71-2385); **Ti** - Titanite, $CaTiSiO_5$ (#25-177); vtg - vestigial content

Table 3 Semi-quantitative normalized chemical analysis (wt%) obtained by XRF-WDS, of incrustations and altered rock from 2014-15 eruption of Fogo volcano, Cape Verde. Sample reference and description are simplified

	F8	F9		F11		F12				F13	F14		F17	F18		F19	F20	F24	F25		F26	F27	
	Whit. hyal. powd.	S aggr.	White incrus.	S aggr.	White powd.	White aggr.	Powd. from rock	Gyp?	S aggr.	S hyal.	S green	Red rock	White incrus.	White aggr.	White powd.	Round white cryst.	White opaq. cryst.	White powd.	White aggr.	White powd. disag.	White powd.	White incrus. hygr.	Yell. incrus.	White powd. (dry)	Yell. incrus.	Oran. incrus.
Na			8.9									2.8	18.1	5.1				32.8			34.3	25.2	15.6	26.4	1.1	9.5
Mg			4.2	0.1	0.7		0.6				0.3	4.5	8.9	6.7	0.7	0.5	1.0			0.4	0.2	4.8	4.9	3.8	1.9	3.1
Al	1.3		15.6	0.1	1.3	1.2	2.0	0.3	0.2	0.4	0.6	15.2	1.2	15.5	2.2	1.6	4.7	1.0	0.1	1.7	0.3	0.3	0.4	0.3	5.2	25.4
Si	5.5		2.8	0.2	3.5	9.0	52.9	6.3	1.5	0.5	6.1	31.9	0.7	1.5	3.4	5.0	79.1	1.2	4.1	26.5	0.3	0.2	0.3		60.3	2.8
P							0.8					0.7											1.9			
S	34.9	100.0	59.9	99.6	36.4	29.7	17.6	32.2	94.4	97.8	89.9	0.9	49.8	66.2	28.5	31.0	5.2	20.5	33.5	34.8	41.9	43.0	40.8	42.1	0.4	0.5
Cl											0.9	1.7	0.9		0.8		1.3	39.5		0.3	17.9	5.0	4.2	5.8	9.0	2.9
K	0.8		2.8		1.0	1.3	1.4	0.2	0.1		0.3	4.5	17.9	1.5	1.0	0.8	0.6	2.5	0.1	0.4	4.0	19.8	27.2	20.7	1.4	10.3
Ca	56.3		2.9		53.7	51.5	7.5	59.1	3.7	1.3	0.7	13.6	0.9	0.9	58.5	55.4	2.6	2.0	56.5	26.7	0.7	0.6	3.0	0.3	7.4	23.5
Ti			0.4		0.5	1.6	9.4	0.9	0.1		0.6	5.3	0.3	0.3	1.0	1.3	4.0		5.0	7.7	0.1				7.9	3.0
V												0.2														0.1
Mn			0.4				0.1					0.3	1.0	0.9								0.9	1.2	0.5	0.2	0.6
Fe	1.3		1.9		2.8	5.4	7.1	0.8			0.5	18.1	0.4	1.3	3.5	3.6	1.4	0.6		1.4	0.1	0.1	0.5		5.1	17.5
Ni												0.1											0.1			
Zn														0.1												
Se																										0.1
Sr					0.1	0.2		0.3							0.5	0.8			0.6	0.1						0.3
Zr							0.1																			0.1
Ba							0.2																			
Ce							0.3																			
Tl																										0.2

aggreg - aggregate; cryst - crystals; disag - disaggregate; gyp - gypsum; hyal - hyaline; hyg - hygroscopic; incrus - incrustations; opaq - opaque; oran - orange; powd - powder; whit - whitish; yell - yellow